Available online at www.sciencedirect.com
ScienceDirect
Ceramics International 37 (2011) 1731–1737
CERAMICS INTERNATIONAL
www.elsevier.com/locate/ceramint

EBSD- and CT-analyses for phase evolution and crack investigations of thermal shocked flame sprayed alumina and alumina-rich structures

P. Gehre *, C.G. Aneziris

Institute of Ceramics, Glass and Construction Materials, TU Bergakademie Freiberg, Agricolastraße 17, 09596 Freiberg, Germany

Received 29 September 2010; received in revised form 9 January 2011; accepted 24 January 2011
Available online 18 February 2011

Abstract

Due to the combination of lamellar structures composed of splats with special Al_2O_3–TiO_2–ZrO_2-compositions free-standing flame spraying coatings with a unique structure were produced. Because of thermal shock treatment, phase and crack evolution takes place. With the aid of EBSD- and CT-method the lamellar structure, the phase transition and the crack evolution were investigated and the prospect of these methods evaluated.

Keywords: D. Flame sprayed alumina; Macro cracks; EBSD; CT

1. Introduction

The microstructure and properties of thermal sprayed alumina-rich ceramic coatings have been extensively investigated due to their potential benefits as thermal barrier coatings as well as in abrasive and sliding wear applications [1–3]. Due to the thermal spray processing it is well known that non-equilibrium γ-Al_2O_3 dominates the phase composition and microstructures are formed whose phase morphologies depend on the solidification reactions [4,5]. A lamellar structure composed of splats is observed containing mainly a population of vertical micro-cracks that support the thermal shock resistance of the coatings [6].

Shi et al. describe the microstructure and the thermal shock behaviour of flame sprayed alumina coatings containing 1.6–2.0% TiO_2 [7]. Bending tests and thermal shock tests by quenching from 1000 to 0 °C in water had been carried out. The structure of the coating could be considered to be a weak joining structure with micro-cracks between lamellar structures composed of splats, like materials constructed of many tiles [7]. According to Shi et al. one method for improving the thermal shock resistance of a coating is by increasing the fracture strain of the coating, considering the important effect of grain size on the fracture strain.

Large residual stress in the coating system due to misfit of Young's modulus of elasticity and thermal expansion coefficient between the ceramic flame sprayed coating and the substrate material decrease the thermal shock performance especially during thermal cycling process [8,9]. Existing researches indicate that functionally gradient structure from bond coat to top coat of thermal sprayed ceramic coating system improves its thermal shock resistance [10].

In a recent work of Damani et al. was shown that heat treatment of bulk plasma sprayed alumina samples induced changes in the strength, fracture and thermal shock characteristics of this material [11]. Bulk plasma spraying Al_2O_3 produces a material with a defect rich ''splat-internal'' microstructure and a non-equilibrium phase composition which are both subject to extensive change by heat treatment. The as sprayed ''intrasplat'' defect structure provides low energy paths for crack propagation. This results in low strength in the range of 20 MPa, but excellent thermal shock resistance. Heat treatment increases overall porosity, but heals the defect structure and increases ''splat'' integrity, leading to a large increase in strength, accentuated R-curve – behaviour and a disproportionate increase in toughness, but also reduction in thermal shock resistance [11].

Aneziris et al. describe the improvement of the thermal shock behaviour of sintered honeycomb structures based on fine grained alumina with additions of MgO partially stabilised ZrO_2 and TiO_2. After sintering besides the Al_2O_3-matrix three additional zones can be identified: zone 1 is a ZrO_2-rich area

* Corresponding author. Tel.: +49 3731 394256; fax: +49 3731 392419.
E-mail address: patrick.gehre@ikgb.tu-freiberg.de (P. Gehre).

0272-8842/$36.00
doi:10.1016/j.ceramint.2011.01.032

covered by a TiO_2-rich zone 2 and a ZrO_2–Al_2O_3–TiO_2-rich zone 3 [12].

All these investigations have been done at coatings or samples, which were produced with different technologies, like flame spaying, plasma spraying or extrusion. It should be considered, that the properties of the structures with similar compositions were different and thus the behaviour under thermal shock is even more different, which makes it hard to compare the above listed results.

In a previous work Aneziris et al. investigated the thermal shock performance of free-standing flame sprayed coatings based on various compositions of the pseudo ternary system Al_2O_3–TiO_2–ZrO_2 according to a Hasselman approach by plotting the residual strength as a function of the temperature gradient [13]. Thus the formation of a high population of microcracks during the flame spraying process leads to coatings with superior thermal shock properties. Furthermore high interconnections of smaller microcracks with the main propagating cracks could be obtained. Because of these interconnections the major propagating cracks will be stabilized and hence slow crack growth during thermal shock is the result. The phase identification of the as sprayed and as shocked coatings was done by XRD and EBSD and the pore structure was investigated with the aid of CT. Unfortunately with the available technique and experiences at this time no appreciable differences between the phases and structures of as sprayed and as shocked coatings were visible.

In terms of this paper the main task of this work is to present improved results of the phase analysis of the alumina-rich coatings before and after thermal shock with the aid of EBSD-method to clarify the phase evolution of the major constituent alumina during thermal shock. Furthermore the lamellar structure and the crack structure before and after thermal shock were investigated with the EBSD and CT-method.

2. Materials and methods

To determine the phases and structure before and after thermal shock free-standing rod flame sprayed coatings were produced according to a basic Al_2O_3–TiO_2–ZrO_2-composition as listed in Table 1, with pure Al_2O_3 as reference.

To feed the flame spraying gun with rods, the raw materials were mixed in advance with a thermoplastic injection moulding binder (Siliplast HO, Zschimmer&Schwarz, Koblenz, Germany) and extruded in a heatable twin screw extruder from Brabender® OHG (Duisburg, Germany). The ceramic raw materials were alumina CT3000SG (Almatis GmbH, Frankfurt, Germany), rutile Tronox TR (Kerr-McGee, Oklahoma City, United States) and monoclinic zirconia (Unitec Ceramics, Stafford, United Kingdom). After partial debinding in water the rods were sintered at 1450 °C to achieve acceptable mechanical strengths for handling during the spraying process. Table 2 presents the parameters of the flame spray process. A MasterJet flame spray gun (Rokide® Spray Unit, Saint-Gobain, Avignon, France) was used. Because of the high combustion temperature of the oxygen–acetylene-mixture of about 3160 °C, the rod will be melted and the melted drops were removed with the aid of compressed air. While flowing a distance of 100 mm towards a substrate the fluidized materials were getting homogenized. By impacting on the substrate the droplets were solidified with an approximate cooling rate of 10^6 K/s. As a result of the high cooling rate high temperature phases were frozen and micro-cracks were initiated. Due to lamination of the droplets coatings were formed. The samples were sprayed through a metallic stencil on a steel substrate coated with soot. This way was chosen to achieve free-standing coatings with dimensions 40 mm (length) × 10 mm (width) × 0.8 mm (thickness). Because of the very low adhesion the coatings could be peeled off with applying nearly no force in such a way minimizing the influence on the structure. This is important because every change in the structure, like micro-cracks, unmelted grains or pores has influences on the thermo-mechanical properties of the coating on which the thermal shock behaviour depends. The main properties are the strength and the Young's modulus of elasticity. Macrocracks, unmelted grains and pores reduce the strength and the thermal shock behaviour. In contrast structures with micro-cracks and no unmelted grains or pores reduces the Young's modulus and improves the thermal shock behaviour. Of each samples the phases and structure were investigated before and after quenching from 700 °C and 1100 °C in water (25 °C) respectively.

Table 1
Compositions of flame sprayed coatings.

Recipe	Al_2O_3 (wt.%)	TiO_2 (wt.%)	ZrO_2 (wt.%)
100:00:00	100	0	0
90:05:05	90	5	5

Table 2
Parameters of the spray process.

Flow of oxygen gas (m^3/h)	3.5
Flow of acetylene gas (m^3/h)	0.8
Flow of air (m^3/h)	28
Gun-to-substrate distance (mm)	100
Rod feed rate (mm/min)	80

Polished surfaces of the obtained microstructures have been characterized by scanning electron microscopy SEM/FEI PHILIPS Type XL30 and electron backscatter diffraction techniques (EBSD). Therefore an area of each composition has been selected, scanned and automatically interpreted.

The characterization of the structure as well as the crack morphology of the as sprayed and thermal-shocked coatings was investigated by 3D-image processing of X-ray tomography with the aid of an Alpha Computer Tomograph of Procon X-ray (Garbsen, Germany). This apparatus is equipped with two high power X-ray guns 160 and 225 kV respectively as well as two X-ray detectors (2048 pixel × 2048 pixel). Through special positioning of the sample between the X-ray gun and the detector voxel sizes of 5.9 μm could be realised. This is the edge length of the smallest detectable volume element within the sample. Disturbance-free information about the micro-structure throughout the volume could be obtained. Detailed descriptions of this technique can be found in Maire et al. [14].

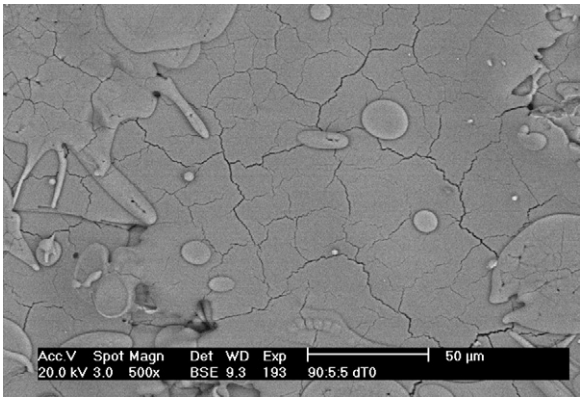

Fig. 1. SEM micrograph of as sprayed composition 90:05:05, two micro-crack patterns.

3. Results and discussion

3.1. SEM of as sprayed and as shocked surfaces

Fig. 1 presents the surface of composition 90:05:05 as sprayed and Fig. 2 quenched with $\Delta T = 700$ K. In Fig. 1 two different micro-crack patterns can be identified. A primary pattern with major propagating cracks with widths between 150 and 300 nm is partially interconnected with a secondary pattern with micro-cracks in the range of 120 nm and less. This secondary micro crack pattern results of slow crack growth during the first thermal shock of the droplets after solidifying on the substrate. The micro-cracks and the branched cracks containing in the as sprayed samples predetermined the developing of the later macro cracks. In Fig. 2 as a result, after thermal shock tests a partial interconnection between the two micro-crack patterns is registered as well as isolated small microcracks of the secondary pattern can be identified.

Hence during thermal shock the energy is expended in extending this secondary micro-crack pattern and the expanse of the propagating major crack is thus restrained. The more secondary cracks will be created during thermal shock the better will be the thermal shock behaviour of the coating.

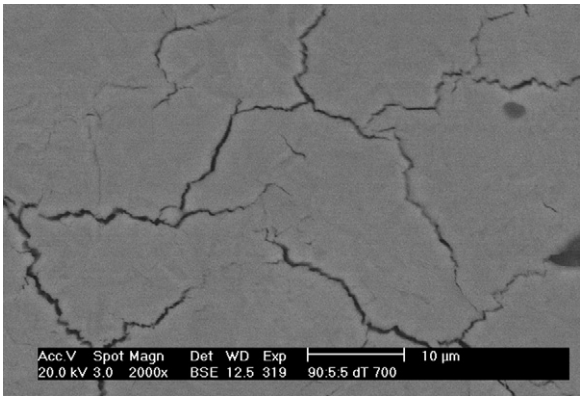

Fig. 2. SEM micrograph of as quenched with $\Delta T = 700$ K composition 90:05:05.

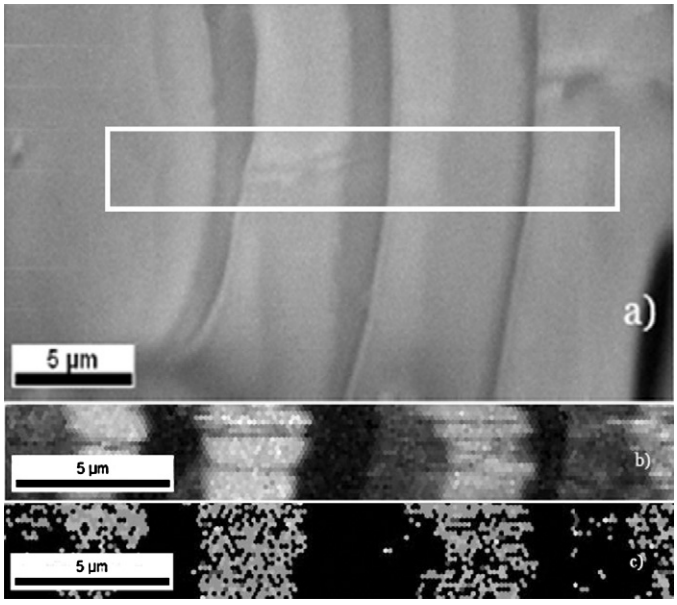

Fig. 3. (a) SEM micrograph of the polished as sprayed composition 90:05:05 with marked area for EBSD, (b) pattern-quality-image: black – no gathered pattern, white – very good pattern quality and (c) interpretation of the Kikuchi pattern: grey – γ'-Al_2O_3; dark grey – α-Al_2O_3; white – $Zr_5Ti_7O_{24}$; black – no interpretation possible.

3.2. EBSD—electron backscatter diffraction

For the EBSD investigations polished cross sections of as sprayed and thermal shocked materials with an additional electrical conductive coating were used. Diffraction patterns can be detected from regions of 10 to 100 nm size directly beneath the surface of the samples. A typical area of about 5 µm times 20 µm was scanned (Fig. 3) and diffraction pattern were carried out. Each diffraction pattern was compared with calculated patterns for all phases according to the phases as listed in Table 3. In all compositions the lattice of some grains was deformed due to the spray processing. Deformation was also introduced due to the preparation process of the samples. Furthermore, there are identical diffraction patterns for certain crystal orientations especially in the case of tetragonal and cubic lattices. Therefore a part of the patterns could not be identified clearly. The results are given in Table 4 while Figs. 4 and 5 demonstrate typical Kikuchi patterns of γ'-Al_2O_3 and cubic ZrO_2 with the corresponding bands and crystal orientations of composition 90:05:05. According to Table 4 and Fig. 3c the main phase of both compositions is a slight deformed cubic alumina. Furthermore corundum, zirconium titanate and no Al_2TiO_5 was identified in the compositions with TiO_2- and ZrO_2-additions.

In Fig. 3 the SEM-Image of the as sprayed composition 90:05:05 shows brighter and darker areas in the lamellar structure which take turns. Again the EBSD-method is a good tool to investigate this lamellar structure. Therefore the quality of the Kikuchi pattern was evaluated and assigned to a grey scale value (Fig. 3b). A white spot indicates a very good pattern quality at this point. A black spot means that there is no Kikuchi pattern detectable which indicates that a pore, a grain boundary

Table 3
Lattice parameters of the phases under consideration for EBSD.

Phase	Crystal system	Lattice param.	
		a, b, c (Å)	α, β, γ (°)
α-Al_2O_3	Trigonal	4.760	90
		4.760	90
		12.99	120
γ-Al_2O_3	Cubic	7.948	90
		7.948	90
		7.948	90
γ'-Al_2O_3	Cubic	7.910	90
		7.910	90
		7.910	90
δ-Al_2O_3	Tetragonal	7.943	90
		7.943	90
		23.50	90
ZrO_2	Monoclinic	5.1507	90
		5.2038	99.196
		5.3156	90
ZrO_2	Tetragonal	5.09	90
		5.09	90
		5.18	90
ZrO_2	Cubic	5.09	90
		5.09	90
		5.09	90
TiO_2	Tetragonal	4.5933	90
		4.5933	90
		2.9592	90
$Zr_5Ti_7O_{24}$	Orthorhombic	5.3255	90
		14.374	90
		5.0236	90
$ZrTiO_4$	Orthorhombic	5.0358	90
		5.4874	90
		4.8018	90
$Zr_5Al_3O_{0.34}$	Hexagonal	8.248	90
		8.248	90
		5.706	120
Al_2TiO_5	Orthorhombic	9.439	90
		9.647	90
		3.5929	90

or an amorphous phase could take place at this point. A grey spot means that there is a bad pattern quality which makes it hard to assign the pattern to a phase. With this acknowledgment, Fig. 3b also gives additional information about the structure of the flame sprayed coating. In the case of the as sprayed samples the black areas indicates amorphous phases. So in the as sprayed coatings there are crystalline areas predominantly composed of γ'-Al_2O_3 and amorphous interlayers in the lamellar structure which take turns.

To investigate the influence of the thermal shock to the phase evolution and the structure, the composition 90:05:05 as

Table 4
Phase identification by EBSD.

Sample	Identified phases
$100{:}00{:}00_{\Delta T=0\ K}$	γ'-Al_2O_3, α-Al_2O_3
$100{:}00{:}00_{\Delta T=1100\ K}$	γ'-Al_2O_3, α-Al_2O_3
$90{:}05{:}05_{\Delta T=0\ K}$	γ'-Al_2O_3, α-Al_2O_3, $Zr_5Ti_7O_{24}$
$90{:}05{:}05_{\Delta T=700\ K}$	γ'-Al_2O_3, α-Al_2O_3, δ-Al_2O_3

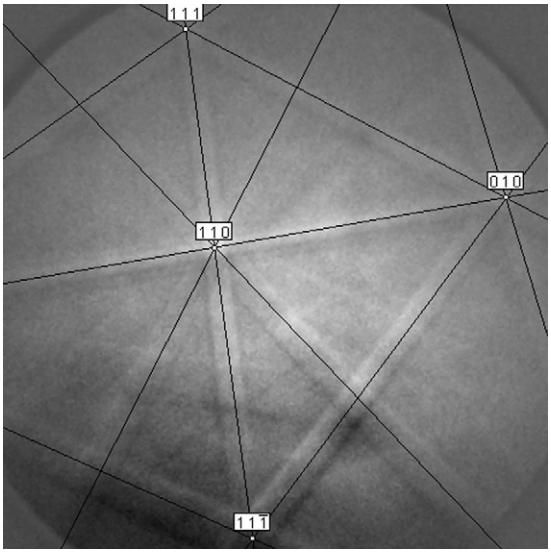

Fig. 4. Typical Kikuchi diffraction pattern of γ'-Al_2O_3 and corresponding simulation (composition 90:05:05).

quenched in water with $\Delta T = 700$ K was examined. Fig. 6a shows a SEM image of the 700 K shocked composition 90:05:05 with marked area for EBSD over an obvious amorphous interlayer. Fig. 6b illustrates the corresponding pattern-quality-image which gives information about the structure. According to this figure only a few amorphous phases but five grains and their grain boundaries are visible.

The interpretation of these Kikuchi pattern in Fig. 6c indicates that the great grains consist of γ'-Al_2O_3 (grey). Between these γ'-Al_2O_3-grains there are some α-Al_2O_3 (light grey) and δ-Al_2O_3 (white) phases detectable. So be caused by the thermal shock based of the amorphous interlayers a phase evolution of γ'-Al_2O_3 over δ-Al_2O_3 to α-Al_2O_3 takes place. The same effect is also visible in the coatings of pure alumina.

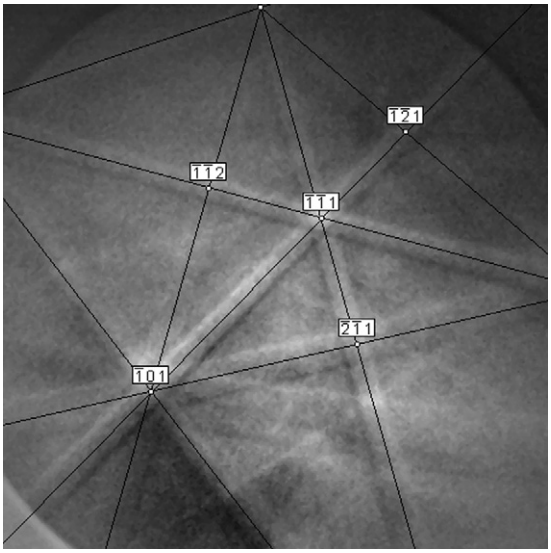

Fig. 5. Typical Kikuchi diffraction pattern of cubic ZrO_2 and corresponding simulation (composition 90:05:05).

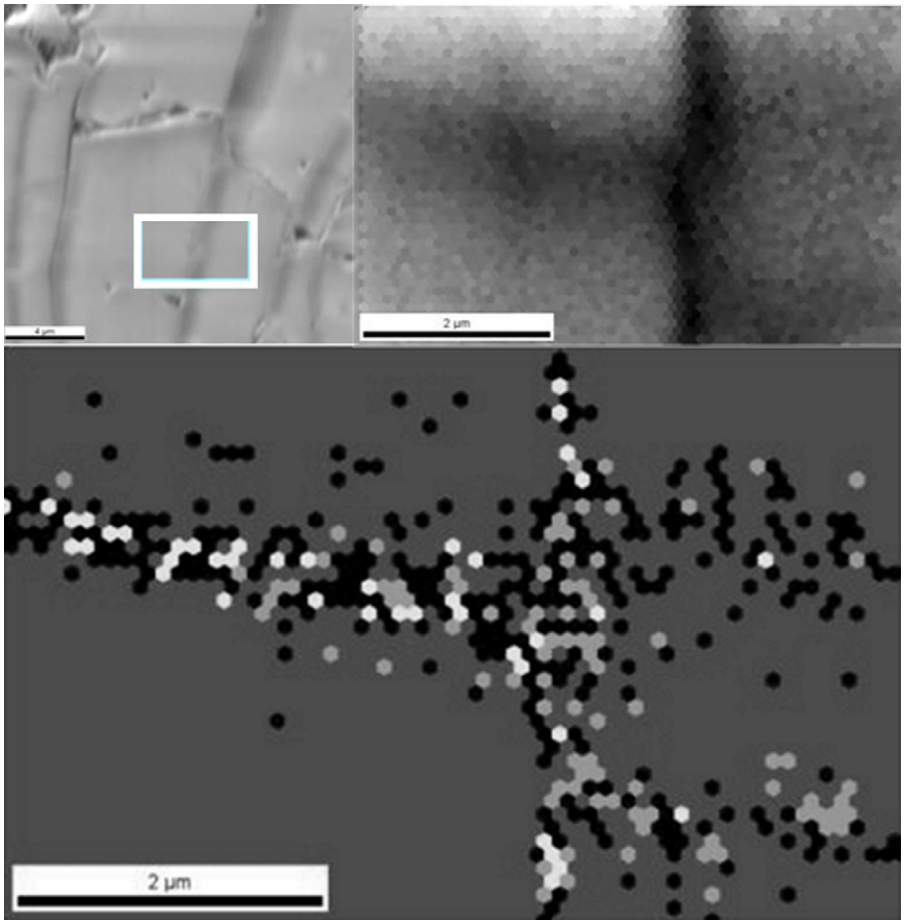

Fig. 6. (a) SEM micrograph of the polished composition 90:05:05, as quenched with a $\Delta T = 700$ K, with marked area for EBSD, (b) pattern-quality-image: black – no gathered pattern; white – very good pattern quality and (c) interpretation of the Kikuchi pattern: black – no interpretation possible; grey – γ'-Al_2O_3; light grey – α-Al_2O_3; white – δ-Al_2O_3.

3.3. Micro X-ray-computer-tomography

Stripes of about 3 mm width and 10 mm length were cutted out of the sprayed layers using a diamond wire saw. These stripes were investigated in the Micro-X-ray-Computer-Tomograph to evaluate the prospect of the CT-method to verify macro-cracks and give information about their spatial distribution before and after thermal shock. The acceleration Voltage of the X-ray source used was 150 kV. Geometrical conditions and point resolution of the detector led to a minimum edge length of the detectable volume element of 5.9 µm (voxel). Typical results are given in Figs. 7 and 8. As a result of a reconstruction process computer tomography yields the spatial distribution of X-ray absorption coefficients. The grey-value presentations show the distribution of X-ray-absorption coefficients on the surfaces of the volume fractions. These pictures are comparable with corresponding cross sections. In the semi-transparent presentations distributions of cracks within the volumes clearly can be identified. There are no significant differences in the density between the different compositions. As shown in Fig. 7 no cracks can be observed in the as sprayed state within the given resolution limits of the computer tomography (the right side surface displays the rough sample surface). After thermal shock tests with a temperature gradient of 1100 K fine cracks are detected by the CT (Fig. 8a and b). These cracks starts from the surface and branching in the inside volume structure, which could be demonstrated with the help of two-dimensional images at different distance from the bottom side of the coating (Fig. 9). So there are no cracks visible in the as sprayed pure alumina and alumina-rich coatings. As it is also shown by Aneziris et al. [13] fine micro-cracks are only detectable in the samples containing TiO_2 and ZrO_2 quenched with a temperature gradient above 600 K. In

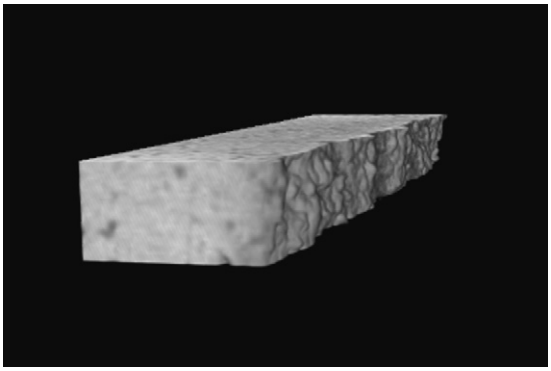

Fig. 7. CT-image of as sprayed composition 100:00:00 (volume fraction 5.6 mm × 1.0 mm × 0.6 mm).

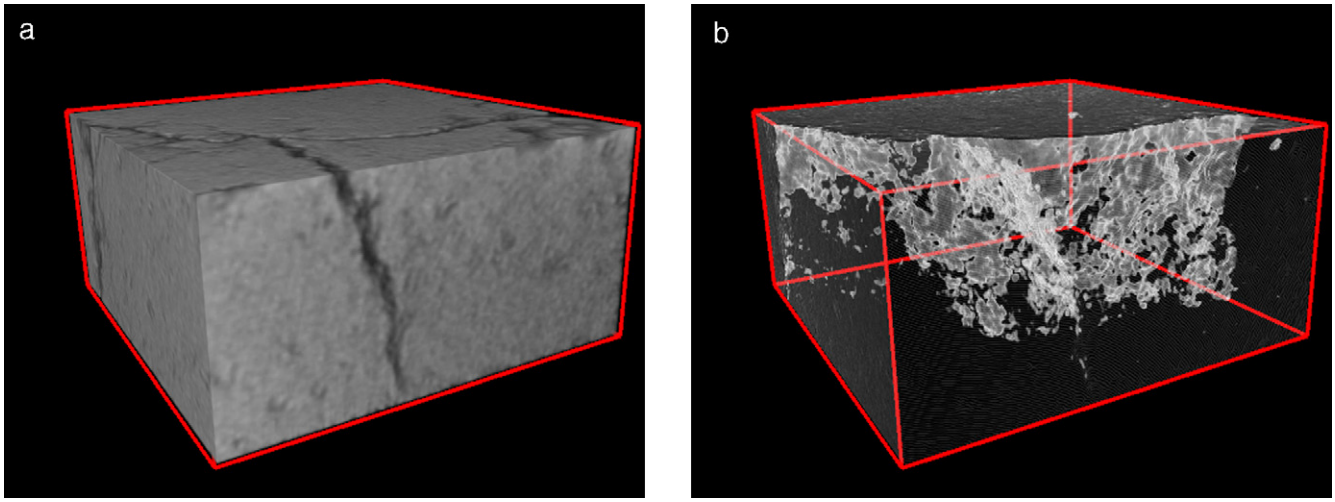

Fig. 8. (a) CT-image of the periphery of the composition 100:00:00 as quenched with a $\Delta T = 1100$ K (volume fraction 1.0 mm × 1.0 mm × 0.5 mm), (b) 3D-image of the cracks in the composition 100:00:00 as quenched with a $\Delta T = 1100$ K (volume fraction 1.0 mm × 1.0 mm × 0.5 mm).

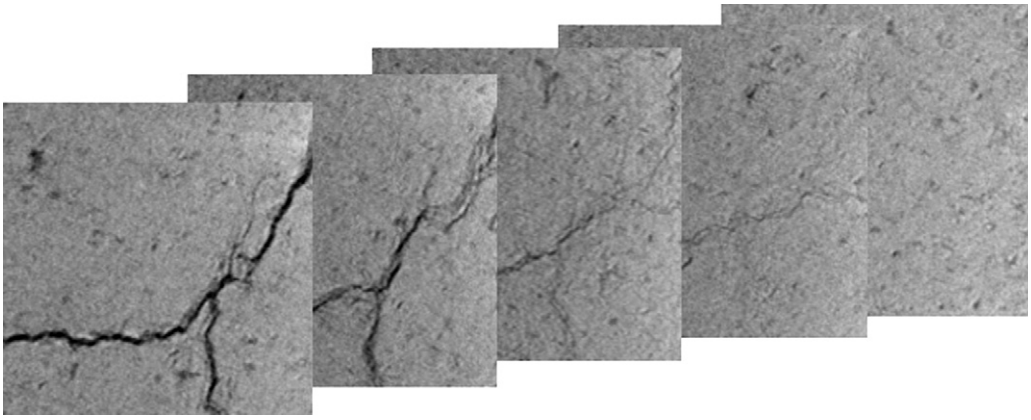

Fig. 9. Two-dimensional images of the coating 100:00:00 quenched with a $\Delta T = 1100$ K showing cracks branching from the surface (left) in the inside volume structure (right) (volume fraction 1.0 mm × 1.0 mm, crack width about 15 μm in the upper area).

contrast in the pure alumina coating there are micro-cracks visible after quenching gradients of about 1000 K.

4. Conclusions

The EBSD-technique is recommended for an improved interpretation of the phase formation especially in materials with high deformed crystal lattices out of high energy processing routes such as the thermal spray processing. With the aid of the EBSD-method a phase evolution of γ'-Al_2O_3 over δ-Al_2O_3 to α-Al_2O_3 based of the amorphous interlayers of the alumina-rich coatings caused by the thermal shock could be detected. The same effect is also visible in the coatings of pure alumina.

The Computer Tomography is a powerful tool for 3D-images, whereby its resolution is directly connected with the power of the X-ray gun, the geometry of the sample, the pixel numbers of the detector and especially the size and the density of the flaws and/or phases that have to be identified. So it is possible to display macro cracks with widths about 10–15 μm as they occur after thermal shock with a quenching temperature of about 600 K in the alumina-rich coating and about 1000 K in the coating composed of pure alumina. At quenching temperatures below about 600 K, the generated cracks are too small to be detectable with the CT-method. CT-images show the evolution of macro cracks of alumina coatings caused by thermal shock, in which the cracks starts from the surface and branching in the inside volume structure. This functionally gradient structure also improves the thermal shock resistance of flame sprayed coatings.

References

[1] E. Lugscheider, Present overview of thermal spraying technology, Schweissen & Schneiden, vol. 54, 2002, pp. 64–67.
[2] G.E. Kim, Thermal sprayed nano-structured coatings: applications and developments, Nanostruct. Mater. (2nd edition) (2007) 91–118.
[3] K.A. Habib, J.J. Saura, C. Ferrer, M.S. Damra, E. Giménez, L. Cabedo, Comparison of flame sprayed Al_2O_3/TiO_2 coatings: their microstructure, mechanical properties and tribology behaviour, Surf. Coat. Technol. 201 (2006) 1436–1443.
[4] D. Fargeot, D. Mercurio, A. Dauger, Structural characterization of alumina metastable phases in plasma sprayed deposits, Mater. Chem. Phys. 24 (1990) 299–314.
[5] W.J. Lackey, D.P. Stinson, G.A. Gerny, L.L. Fehrenbacher, A.C. Schaffhauser, Ceramic Coatings for Heat Exchange Engine Materials – Status

Future ORNL/TM-8959, Oak Ridge National Laboratory, Oak Ridge, TN, 1985.

[6] L. Shindle, D.A. Olson, L.C. De Jonghe, R.A. Miller, Degradation mechanisms in thermal-barrier coatings, Ceram. Eng. Sci. Proc. 7 (7–8) (1986) 1032–1038.

[7] K.S. Shi, Z.Y. Qian, M.S. Zhuang, Microstructure and properties of sprayed ceramic coating, J. Am. Ceram. Soc. 71 (11) (1988) 924–929.

[8] E. Tzimas, H. Mullejans, S.D. Peteves, J. Bressers, W. Stamm, Evaluation of interfacial mechanical properties under shear loading in EB-PVD TBCs by the push out method, Acta Mater. 4 (8) (2000) 4699–4707.

[9] X. Jiang, Y. Wan, H. Herman, S. Sampath, Role of condensates and adsorbates on substrate surface on fragmentation of impinging molten droplets during thermal spray, Thin Solid Films 385 (2001) 131–141.

[10] A. Kawasaki, R. Watanabe, Thermal fracture behaviour of metal/ceramic functionally graded materials, Eng. Fract. Mech. 69 (2002) 1713–1728.

[11] R.J. Damani, D. Rubesa, R. Danzer, Fracture toughness, strength and thermal shock behaviour of bulk plasma sprayed alumina—effects of heat treatment, J. Eur. Ceram. Soc. 20 (2000) 1439–1452.

[12] C.G. Aneziris, W. Schärfl, B. Ullrich, Microstructure evaluation of Al_2O_3 ceramics with Mg-PSZ- and TiO_2-additions, J. Eur. Ceram. Soc. 27 (2007) 3191–3199.

[13] C.G. Aneziris, P. Gehre, T. Kratschmer, H. Berek, Thermal shock behaviour of flame sprayed free-standing coatings based on Al_2O_3 with TiO_2- and ZrO_2-additions, Int. J. Appl. Ceram. Technol., in press.

[14] E. Maire, P. Colombo, J. Adrien, L. Babout, L. Biasetto, Characterization of the morphology of cellular ceramics by 3D image processing of X-ray tomography, J. Eur. Ceram. Soc. 27 (2007) 1973–1981.